Supporting Online Material

Materials and Methods

Molecular Biology

Cloning of the traN to traF gene cluster for production of a core T4SS complex with a C-terminal Strep-tag on TraF/VirB10. The *tra* operon region encoding *traN* to *traF* was amplified by PCR using oligonucleotides containing BsaI restriction sites at their 5' ends (see Table S1 for sequence of oligonucleotides). The PCR fragment was then cloned into pASK-IBA3c using BsaI DNA restriction and T4 ligase DNA ligation to yield the IBA3c:*traN-traF*$_{C\text{-}ST}$ plasmid ("C-ST" indicates a "C-terminal Strep-tag").

Introduction of a Cys at position 224 in TraO/VirB9 for stoichiometry measurements. The TraO/VirB9 Ser224Cys mutation was introduced using site-directed mutagenesis of IBA3c:*traN-traF*$_{C\text{-}ST}$ as implemented in the QuickChange protocol (Invitrogen; see Table S1 for oligonucleotides), yielding the IBA3c:*traN-traO*$_{Ser224Cys}$-*traF*$_{C\text{-}ST}$ plasmid for production of the TraN/VirB7-TraO/VirB9$_{Ser224Cys}$-TraF/VirB10$_{C\text{-}ST}$ core complex.

Mutation of TraN/VirB7 Cys15 to Ser. The TraN/VirB7 Cys15Ser mutation was introduced using site-directed mutagenesis of IBA3c:*traN-traF*$_{C\text{-}ST}$ as implemented in the QuickChange protocol (Invitrogen; see Table S1 for oligonucleotides), yielding the IBA3c:*traN*$_{Cys15Ser}$-*traF*$_{C\text{-}ST}$ plasmid for production of the TraN$_{Cys15Ser}$/VirB7-TraO/VirB9-TraF/VirB10$_{C\text{-}ST}$ core complex or "ΔL_1" complex.

Deletion of the TraE/VirB8, TraN/VirB7, or TraO/VirB9 gene. The *traN, traE,* or *traO* genes were deleted using deletion mutagenesis of IBA3c:*traN-traF*$_{C\text{-}ST}$ as implemented in the QuickChange kit (Invitrogen; see Table S1 for oligonucleotides), yielding the *traN-traF*$_{C\text{-}ST}$*(ΔtraN), traN-traF*$_{C\text{-}ST}$*(ΔtraE)* and *traN-traF*$_{C\text{-}ST}$*(ΔtraO)* plasmids, respectively.

Deletion of the traF/virB10 gene. To study the role of the TraF/VirB10 protein in assembly of the core complex, it was not possible to start from the IBA3c:*traN-traF*$_{C\text{-}ST}$ clone. This is because our attempts at introducing a tag at the C-terminus of the TraN/VirB7 protein or at either the N- or C-terminus of the TraO/VirB9 protein failed to produce assembly-competent proteins (no core complex was produced). Thus, the only

alternative left was to introduce a tag at the N-terminus of TraN/VirB7. The sequence encoding a fragment of the *traN-traF* cluster differing from the previous one (see above) in that it lacked the sequence encoding the first 18 amino acids of TraN/VirB7 (this excludes the entire signal peptide and the lipidated Cys15) was amplified by PCR (see Table S1 for oligonucleotides used) and cloned into the IBA12 vector. This resulted in the substitution of the 18 first amino acids of TraN/VirB7 with an OmpA signal peptide followed by a Strep-tag, yielding the IBA12:*$_{OmpA,N\text{-}ST}$TraN-TraF* plasmid for production of the $_{OmpA,N\text{-}ST}$TraN/VirB7-TraO/VirB9-TraF/VirB10 core complex or "ΔL_2" complex. The *traF* gene was subsequently deleted as described above for deletion of the *traE*, *traN* or *traO* genes (resulting in the *$_{OmpA,N\text{-}ST}$TraN-TraO* cluster; see Table S1 for oligonucleotides used for deletion).

Addition of the His$_6$-tag to the N-terminus of TraF/VirB10. The sequence encoding a His_6-tag was added to the 5' end of the *traF/virB10* gene using site-directed mutagenesis of IBA3c:*traN-traF$_{C\text{-}ST}$* as implemented in the QuickChange protocol (Invitrogen; see Table S1 for oligonucleotides), yielding the IBA3c:*traN-$_{N\text{-}His}$traF$_{C\text{-}ST}$* plasmid for production of the TraN/VirB7-TraO/VirB9-$_{N\text{-}His}$TraF/VirB10$_{C\text{-}ST}$ core complex.

Core complex expression and purification

Four core complexes were produced and purified using the protocol below: i- the wild-type TraN/VirB7-TraO/VirB9-TraF/VirB10$_{C\text{-}ST}$ complex used for EM imaging of the wild-type core complex; ii- the TraN$_{Cys15Ser}$/VirB7-TraO/VirB9-TraF/VirB10$_{C\text{-}ST}$ core complex termed "ΔL_1" and used to evaluate the role of TraN/VirB7 lipidation; iii- the $_{OmpA,N\text{-}ST}$TraN/VirB7-TraO/VirB9-TraF/VirB10 core complex termed "ΔL_2" and used to subsequently evaluate the deletion of TraF/VirB10 in core complex assembly; iv- the TraN/VirB7-TraO/VirB9-$_{N\text{-}His}$TraF/VirB10$_{C\text{-}ST}$ used to determine the topology of the core complex by anti-His antibody labelling and EM imaging. In addition, the protocol below was used to purify complexes produced by induced *traN-traF$_{C\text{-}ST}$* clusters where the *traN/virB7* (*traN-traF$_{C\text{-}ST}$(ΔtraN)*), *traE/virB8* (*traN-traF$_{C\text{-}ST}$(ΔtraE)*), or *traO/virB9* (*traN-traF$_{C\text{-}ST}$(ΔtraO)*) genes were deleted (see above).

All plasmids were transformed into BL21 strain and protein expression was

induced by addition of 200 µg/l of anhydrotetracyclin during the exponential growth phase. Crude membrane fraction was isolated by ultracentrifugation (100,000g, 45 min) after cells were broken using an emulsiflex-C5 (Avestin). Membrane proteins were solubilized in 50 mM Tris/HCl pH8.0, 50 mM NaCl, 1mM EDTA, 10 mM LDAO (n-dodecyl-n,n-dimethylamine-n-oxide from Anatrace), 1mM DDM (n-dodecyl-β-D-maltopyranoside from Anatrace) and insoluble material was removed by ultracentrifugation. Solubilized proteins were loaded onto a Strep-Tactin sepharose affinity column (IBA). The column was washed with 50 mM TrisHCl pH8.0, 200 mM NaCl, 10 mM LDAO and eluted in the same buffer in which 2.5 mM desthiobiotin (Sigma) was added. The eluted proteins were then concentrated by filtration using a 100 kDa cut-off spin concentrator (Amicon) and loaded onto a superose 6 GL 10/300 (GE Healthcare) gel filtration column in 50 mM TrisHCl pH8.0, 200 mM NaCl, 10 mM LDAO (Fig. 1 in main text). Protein content was analyzed after SDS-PAGE using Nu-PAGE 3-12% gels (Invitrogen) and Coomassie staining (safestain, Invitrogen). The purified proteins eluted as a single peak on the gel filtration column containing 3 proteins that were identified by mass spectrometry fingerprinting as TraF, TraO and TraN. The molecular mass of the complex (1,100 kDa) was deduced from its elution volume compared to those of standard proteins (HMW gel filtration calibration kit, GE Healthcare). Such a molecular mass is similar to that calculated from the molecular weight of the components (see below stoichiometry determination section), indicating that the contribution of bound detergents to the molecular mass is small. The purity of the sample assessed by silver stained acrylamide gels was greater than 95 %.

The TraN/VirB7-TraO/VirB9$_{Ser224Cys}$-TraF/VirB10$_{C\text{-}ST}$ core complex used to evaluate the stoichiometry of the core complex was purified using the same protocol with the exception of the gel filtration step being carried out in a buffer containing 50 mM TrisHCl pH7.0, 200 mM NaCl, and 10 mM LDAO.

For complexes resulting from expression of the $_{OmpA,N\text{-}ST}$*traN-traO* cluster (deletion of *traF/virB10*), as these complexes are soluble (none is found in membrane fraction), they were purified from the soluble fraction using Strep-Tactin affinity chromatography followed by gel filtration as described above (but in the absence of detergents).

TraO/VirB9 – TraF/VirB10 stoichiometry determination. TraN/VirB7-TraO/VirB9$_{Ser224Cys}$-TraF/VirB10$_{C\text{-}ST}$ core complex was purified as described above. The Ser224Cys mutation on TraO did not affect the multimerization state of the complex as the complex had the same apparent molecular mass using gel filtration or BN-PAGE (results not shown). The protein concentration of the sample was set to 0.1 mg/ml. The proteins were denaturated in 1% SDS at 100°C for 10 minutes. The denatured sample was incubated in presence of 40 μM of Alexa Fluor® 532 C5-maleimide (Invitrogen) and 1 mM TCEP (Pierce) during 2h at room temperature. The labeled proteins were separated by SDS-PAGE and protein-bound fluorescence visualized and quantified using a Fujifilm FLA-3000 scanner.

Inner and outer membrane separation. Cells were broken using an Emulsiflex-C5 (Avestin). Crude membrane fraction was isolated by ultracentrifugation (100,000g, 45 min). Bacterial outer and inner membranes were separated by differential detergent-induced solubilization. Inner membranes were solubilized in 50 mM TrisHCl pH8.0, 0.5% sodium N-lauroyl sarcosyl during 30 minutes at room temperature. The insoluble material containing the outer membrane fraction was isolated by ultracentrifugation (100,000g, 20 min). The outer membrane pellet was then solubilized in 50 mM TrisHCl pH8.0, 50 mM NaCl, 1mM EDTA, 10 mM LDAO, 1mM DDM. The insoluble material was removed by ultracentrifugation (100,000g, 20 min).

Surface accessibility studies The method was adapted from a cell surface accessibility assay commonly used on *E. coli* cells (*S1*). Cells (OD_{600}=0.5) were harvested, washed and resuspended with 20 ml of ice-cold phosphate-buffered saline (PBS). Sulfo-NHS-S-S-biotin (Pierce; 0.5 mM final) was added to label the surface exposed lysine residues. After 30 minutes at 4°C, the cells were centrifuged and resuspended in 100 mM TrisHCl pH8.0 to stop the labelling reaction. Cells were then broken using an Emulsiflex-C5 and membranes were isolated by ultracentrifugation. Membrane proteins were solubilized in 50 mM TrisHCl pH8.0, 50 mM NaCl, 1mM EDTA, 10 mM LDAO, 1mM DDM, and insoluble material was removed by ultracentrifugation. Solubilized proteins were mixed

with neutravidin resin (Pierce) and incubated for 30 minutes at room temperature on a shaker. The resin was then washed with 50 mM TrisHCl pH8.0, 200 mM NaCl, 10 mM LDAO. The biotinylated proteins were eluted from the resin by incubation of the resin with 50 mM TrisHCl pH8.0, 200 mM NaCl, 10 mM LDAO, and 150 mM 2-mercaptoethanol for 15 minutes at room temperature (2-mercaptoethanol breaks the disulfide bridge in the Sulfo-NHS-S-S-biotin and leaves the biotin on the neutravidin resin).

Symmetry determination using negative stain electron microscopy. Wild-type, ΔL2, D1 and D2 samples were applied onto glow-discharged, carbon-coated copper grids. The sample was left for 1–2 min on the grids before blotting and staining with a solution of 2% uranyl acetate. Low electron dose images were recorded on film using a Tecnai T12 microscope operating at 120 kV and 42,000X. All micrographs were checked on an optical diffractometer for drift and astigmatism. Micrographs were digitised on a Zeiss SCAI scanner with a step size of 7 μm (1.66 Å/pixel at the specimen level). The digitized images were then reduced by 3x3 pixel averaging to 5 Å/pixel. All these datasets were recorded with a defocus range of 800–2000 nm. For each type of complex (Native, ΔL2, D1 and D2) a total of ~300 particles corresponding to end-views (ring-like structures) were selected from various micrographs. Images were normalised to the same mean and standard deviation and band-pass filtered. Images were centred, subjected to multivariate statistical analysis (MSA) (*S2*), and classified with approximately ten images per class. The rotational auto-correlation function of each class average was calculated and plotted. For each complex, such analysis revealed the presence of 14-fold rotational symmetry. This 14-fold symmetry feature was also present in the eigen-images generated during the MSA analysis of each complex (not shown).

Negative stain EM structures of the wild-type, ΔL2 and D1 complexes. The wild-type, *ΔL2,* and the D1 complexes were stained as above.

For the wild-type complex, charge-coupled device (CCD) images were recorded on a 4,096x4,096 Gatan CCD camera with low electron dose on a Tecnai F20 FEG microscope operating at a voltage of 200 kV, a magnification of 68,100 and a defocus

range of 800–2,500 nm. Adjacent pixels were 2x2 averaged to yield a final pixel size of 4.44 Å. A total of 2,890 particles were selected from 61 CCD images and windowed into 80x80 pixel boxes.

For the D1 complex and ΔL2, low electron dose images were recorded on film using a Tecnai T12 microscope operating at 120 kV and 42,000X with a defocus range of 800–2,000 nm. Micrographs were digitised on a Zeiss SCAI scanner with a step size of 7 μm (1.66 Å/pixel at the specimen level). The digitized images were then 3x3 reduced to 5 Å/pixel. A total of 3,868 particles for D1 and 1,598 particles for ΔL2 were selected from 22 and 15 micrographs respectively and windowed into 100x100 pixel boxes.

For the wild-type, D1 and ΔL2 complexes, images were centred, subjected to MSA, and classified with approximately 10-15 images per class. These images were further aligned and classified by several rounds of multi-reference alignment, where the best classes representing characteristic views, with the lowest intra-class variance, were used as references, followed by MSA. The first 3D reconstruction was calculated by angular reconstitution with 14-fold symmetry using 5 characteristic views of the complex. This first 3D map was then refined with several rounds of anchor set refinement and multi-reference alignment, reducing the number of images per class to five. The final maps for the native, D1 and ΔL2 complexes were respectively calculated from 2,205, 2,201 and 1,231 particles. The 0.5 correlation of the Fourier shell correlation curve indicated a resolution of 18 Å, 19 Å and 18 Å for the native, D1 and ΔL2 complex maps respectively (Fig. S6).

Cryo-EM structures of the native and D2 complexes. The wild-type TraN/VirB7-TraO/VirB9-TraF/VirB10$_{C\text{-}ST}$ core complex (5 mg ml^{-1}) was applied to lacey carbon grids that had been glow discharged for 30 s and was vitrified by plunging into liquid ethane. Images were recorded on a 4,096x4,096 Gatan CCD camera with low electron dose on a Tecnai F20 FEG microscope operating at a voltage of 200 kV, a magnification of 68,100 and a defocus range of 1,250–3,500 nm. Adjacent pixels were 2x2 averaged to yield a final pixel size of 4.44 Å. The effects of the contrast transfer function were corrected by phase flipping and the contrast was inverted. Images with more than 5% astigmatism were discarded. A total of 9,991 particles were selected from 420 CCD images and

windowed into 150x150 pixel boxes.

Images were normalised to the same mean and standard deviation and band-pass filtered: the low-resolution cut-off was ~100 Å to remove uneven background; the high-resolution cut-off was ~8.8 Å. Images were centred, subjected to MSA, and classified initially with approximately 10-15 images per class. The data set was further aligned and classified by several rounds of multi-reference alignment using the best classes as references, followed by MSA. After excluding obviously defective images, a total of 5,619 images were retained for subsequent processing. The first 3D reconstruction was calculated by angular reconstitution using 10 characteristic views of the complex. On the basis of the symmetry observed by negative stain, 14-fold symmetry was applied throughout the procedure. Refinement of this initial map was carried out using anchor set refinement interspersed with rounds of multi-reference alignment and classification reducing the number images per class to five. The final 3D map was calculated from 3,051 particles and had a resolution of 15 Å as determined by Fourier shell correlation at 0.5 correlation (Fig. S6). The map displayed in Figs 2, 3, and 4 and Figs. S4 and S5 was low-pass filtered at 14 Å resolution.

For analysis of the D2 complex by cryo-EM, the same procedure was used. As the resolution of the reconstruction was not crucial for the interpretation, a smaller data set (1,557 particles were selected from 60 CCD images) was used. The final 3D map was calculated from 775 particles and had a resolution of 20 Å as determined by Fourier shell correlation at 0.5 correlation (Fig. S6). The map displayed in Fig. 3 and Fig. S4 was low-pass filtered at 18 Å resolution.

Localization of the TraF/VirB10 N-terminus by anti-His_6 antibody labelling and negative stain electron microscopy. The TraN/VirB7-TraO/VirB9-$_{N\text{-}His}$TraF/VirB10$_{C\text{-}ST}$ core complex was concentrated to 0.5 mg/ml and mixed with monoclonal anti-His_6 antibodies (Sigma) at a core complex:antibody ratio of 2:1. The mixture was incubated at 4°C for 30 minutes and the labelled core complex was isolated by gel filtration. The sample was analysed by negative stain EM as described above for negative stain EM of the wild-type core complex.

Image processing and visualization. Defocus values were determined with the program CTFFIND3 (*S3*). The particles were selected and windowed using the EMAN/BOXER software package (*S4*). Image processing including alignment, statistical analysis, determination of angular orientations by angular reconstitution (*S5*), 3D-reconstruction and structure refinement were performed using IMAGIC-5 (*S6*). Surface rendering was done in Chimera (*S7*). The density threshold for surface rendering was chosen to enclose the volume corresponding to a molecular weight of 1050 kDa for the wild-type complex, 868 kDa for the D1 complex and 602 kDa for the D2 complex. The docking of the *Helicobacter pylori* comB10 crystal structure (pdb entry code: 2BHV) into the cryo-EM map of the wild-type core complex was performed by manual fitting with automated local refinement in Chimera. The best fit was then adjusted using the Flex-EM method (*S8*). Goodness of fit parameter was calculated using SITUS (*S9*).

Fig. S1 Fronzes et al. (2008)

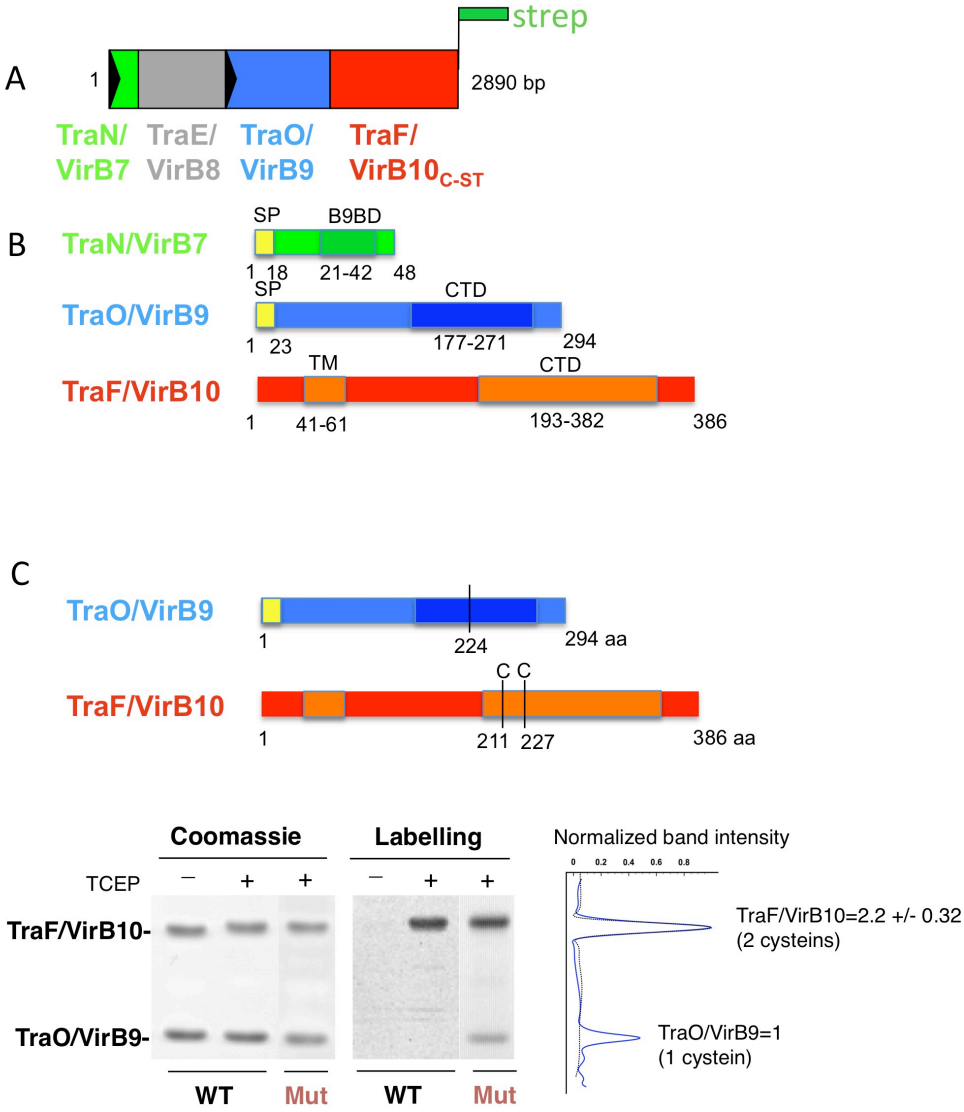

Fig. S2 Fronzes et al. (2008)

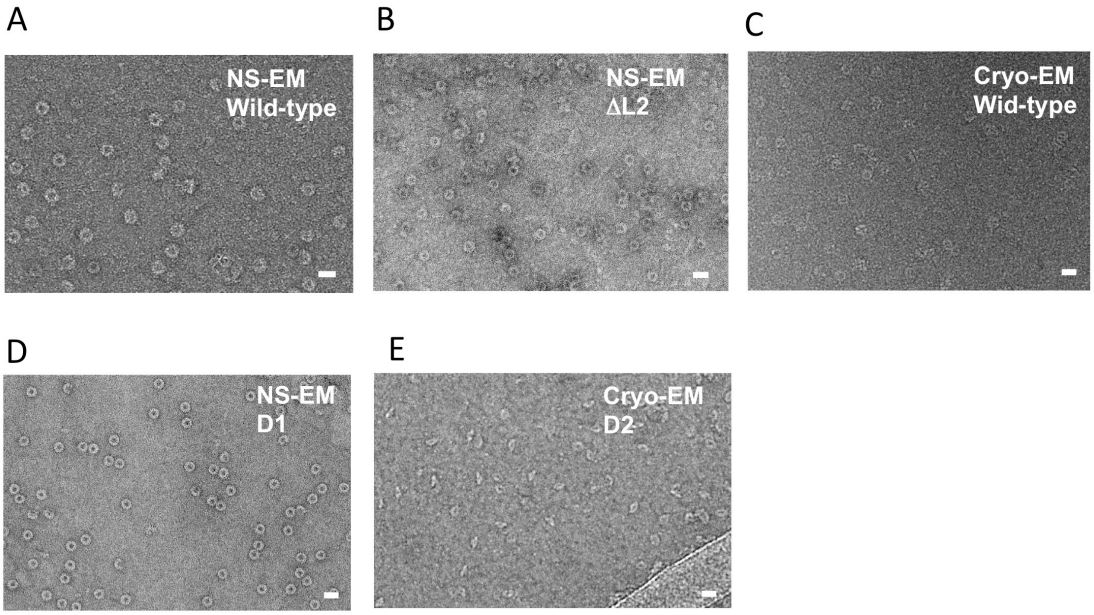

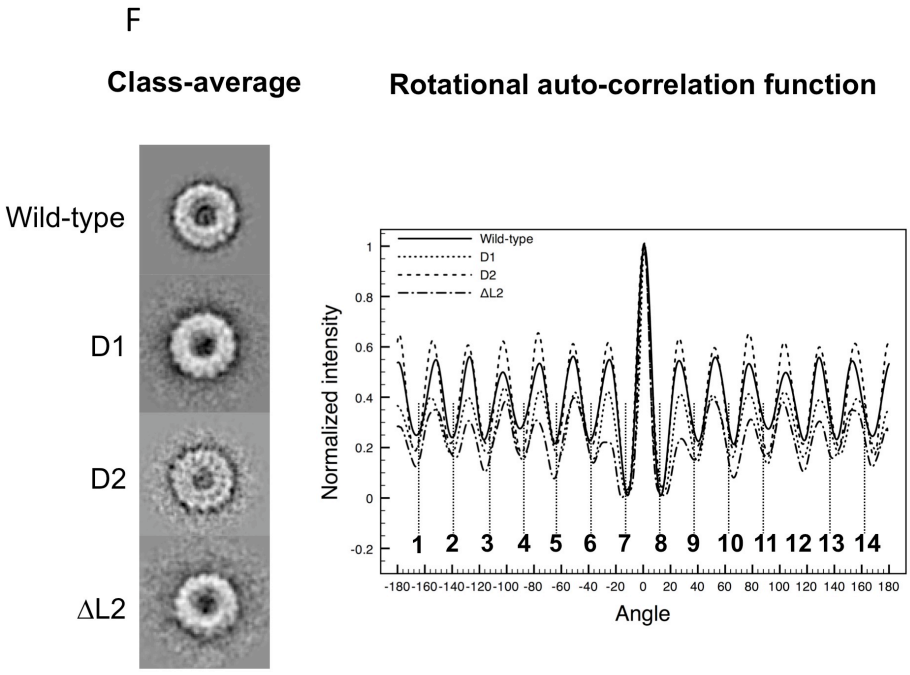

Fig. S3 Fronzes et al. (2008)

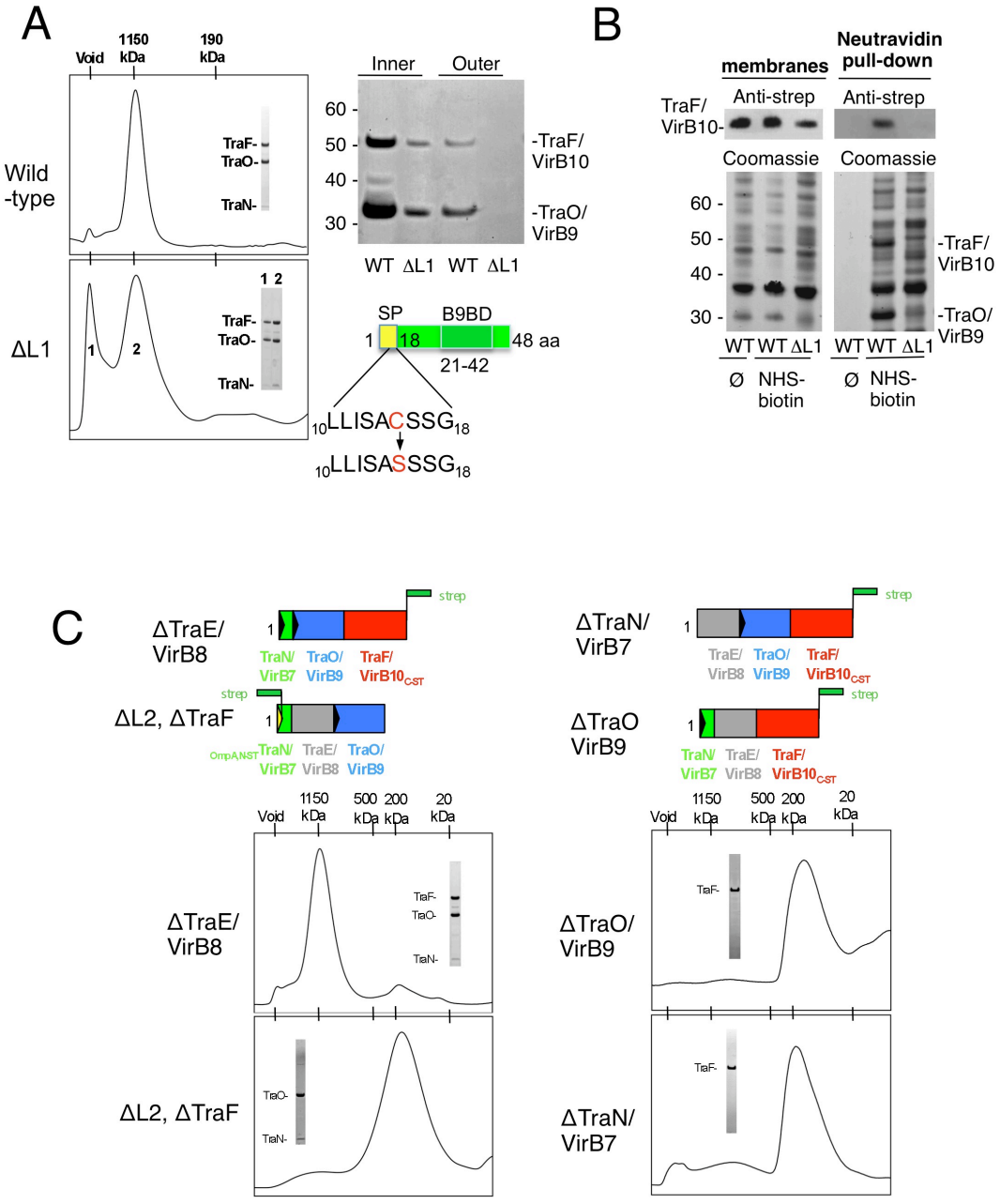

Fig. S4 Fronzes et al. (2008)

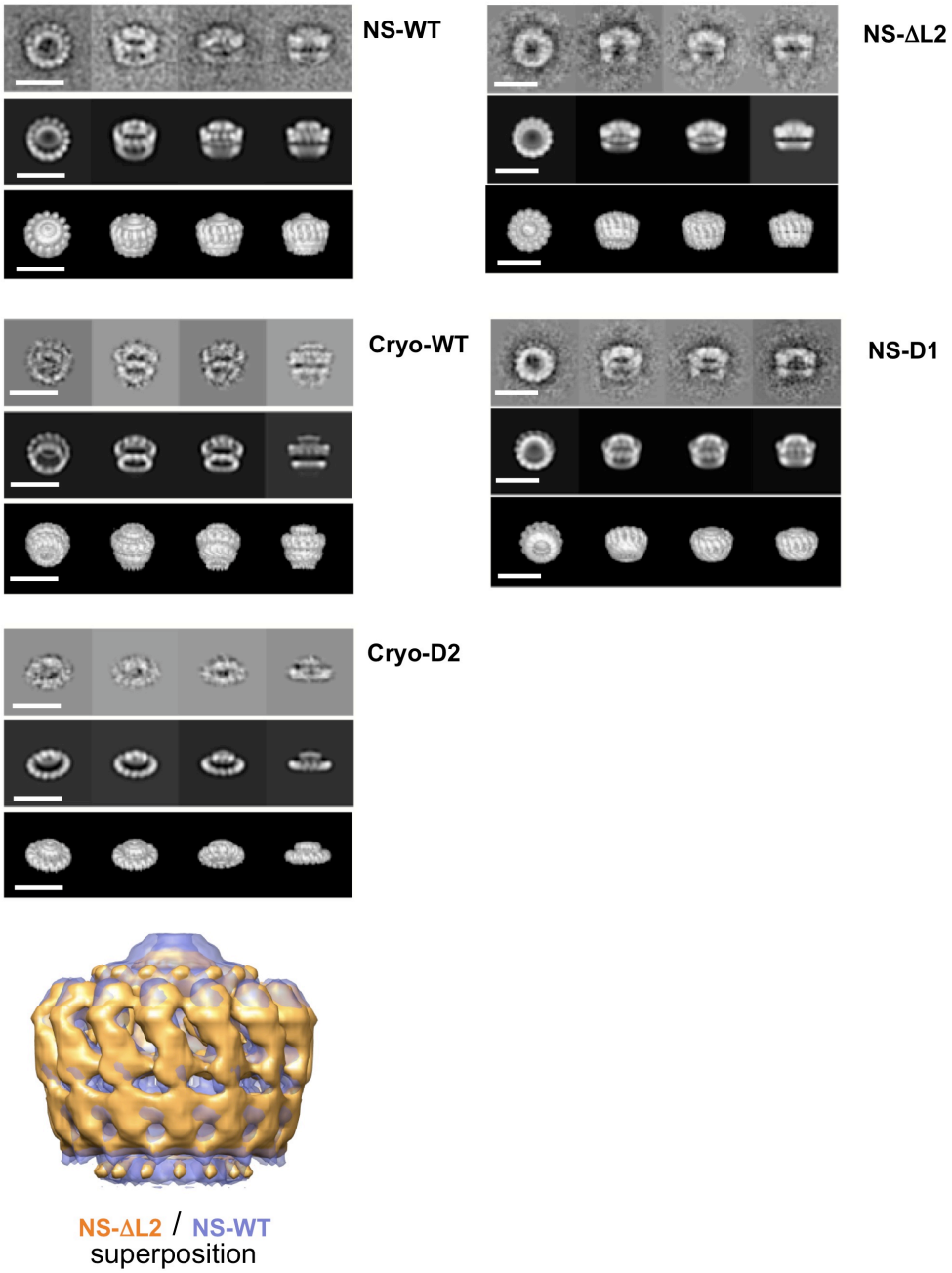

Fig. S5 Fronzes et al. (2008)

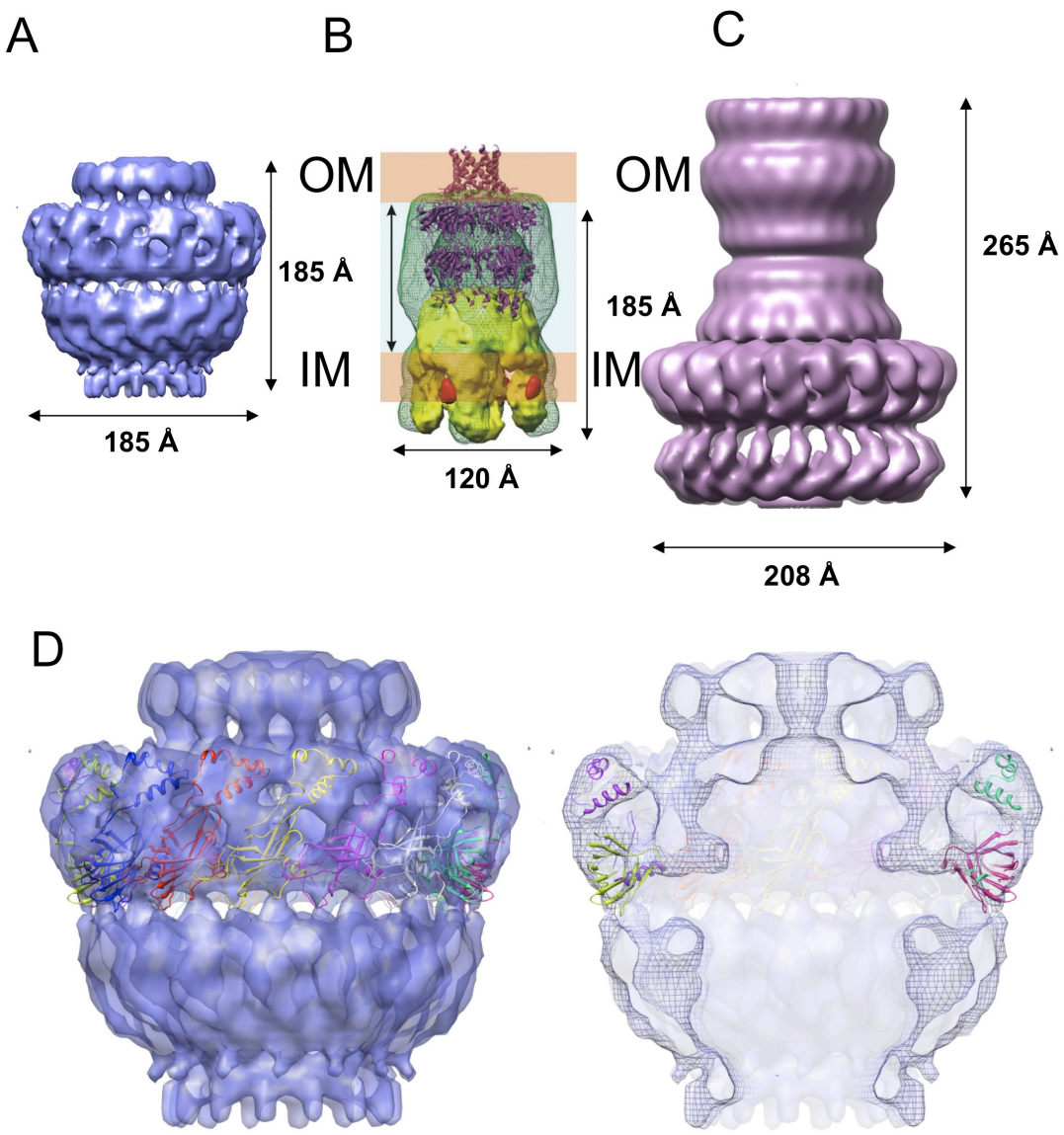

Fig. S6 Fronzes et al. (2008)

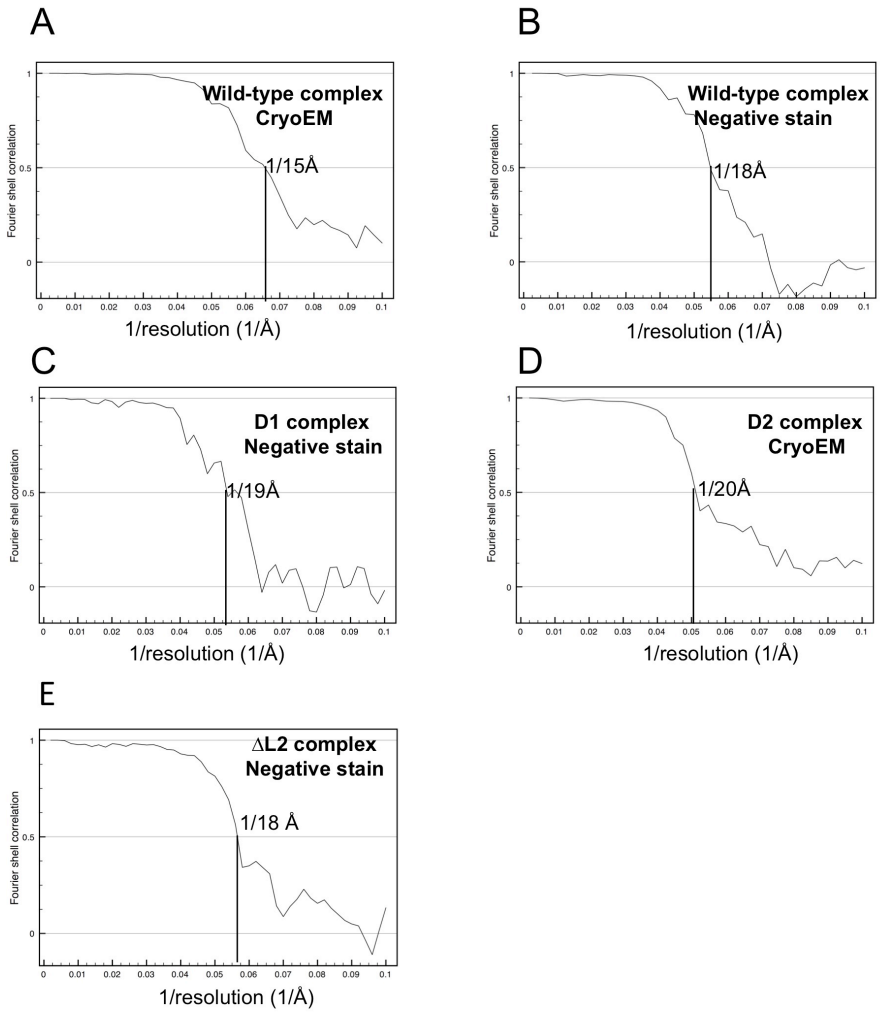

Supplementary Figure legends

Fig. S1. **A.** Construct used for expression of the TraN/VirB7, TraO/VirB9, and TraF/VirB10$_{C\text{-}ST}$ core complex. **B.** Schematic description of the domain structure of TraN/VirB7, TraO/VirB9, and TraF/VirB10. TraN/VirB7, TraO/VirB9 and TraF/VirB10 are respectively 48, 294 and 386 residues long including the signal peptide. TraN/VirB7: residues 1-18 contain the signal sequence targeting the protein to the periplasm and the lipidation site (residue Cys15); the region named B9BD is the region of TraN/VirB7 interacting with TraO/VirB9 (B9 Binding Domain). TraO/VirB9: residues 1-23 targets TraO/VirB9 to the periplasm; the domain named CTD (C-Terminal Domain; residues 177-271) is the C-terminal domain of the protein interacting with TraN/VirB7. TraF/VirB10: a single trans-membrane segment (named TM, residues 41-61) mediates the insertion of the protein in the bacterial inner-membrane; the domain named CTD (C-Terminal Domain; residues 193-382) is the C-terminal domain of the protein, the structure of which is known (*S10*). The structure of the C-terminal domains of TraO/VirB9 in a complex with TraN/VirB7 is also known (*S11*). **C.** Cysteine labelling of TraO/VirB9$_{S224C}$ and TraF/VirB10$_{C\text{-}ST}$. For this experiment, a cysteine was introduced by site-directed mutagenesis at position 224 in TraO/VirB9 (the wild-type protein does not contain any cysteine) and the resulting TraN-TraO$_{Ser224Cys}$-TraF$_{C\text{-}ST}$ core complex was produced, purified, and analysed as described in supplementary Materials and Methods. Upper panel: localization of the cysteine residues in the sequence of TraO/VirB9 and TraF/VirB10. Lower left panel: Coomassie stained SDS-PAGE (labelled “Coomassie”) of wild-type (WT) and mutated (Mut) core complexes labelled with AlexaFluor maleimide in the presence (+) or absence (-) of TCEP. Lower middle panel: fluorescence scanning of the gel at left (before Coomassie staining). Lower right panel: quantification of the fluorescence

scan. These results demonstrate a 1:1 stoichiometry for the TraO/VirB9 and TraF/VirB10 proteins. As it has already been established that TraN/VirB7 and TraO/VirB9 form a 1:1 complex (*S11*), we conclude that the stoichiometry for the wild-type core complex is 1:1:1 of TraN/VirB7, TraO/VirB9, and TraF/VirB10$_{C\text{-}ST}$.

Fig. S2. Electron micrographs and symmetry analysis of the particles. Scale bar: 20 nm. **A.** Negative stain EM of the wild-type core complex. **B.** Negative stain EM of the ΔL2 complex. **C.** Cryo-EM of the wild-type core complex. **D.** Negative stain EM of the D1 complex. **E.** Cryo-EM of the D2 complex. **F.** Symmetry of the wild-type native, D1, D2 and ΔL2 complexes. A representative end-view class-average for each particle type is displayed next to the rotational auto-correlation function graphs.

Fig. S3. Assembly of the core complex **A.** Assembly and membrane localization of the wild-type and ΔL1 mutant. Left panel: gel filtration profile of the purified wild-type and ΔL1 complexes. The two complexes are virtually similar in molecular weight (compare single peak in the wild-type trace and peak 2 in the ΔL1 trace). However, ΔL1 complexes also tend to aggregate (excluded volume peak 1). Insets in each panel show a Coomassie-stained SDS-PAGE analysis of the corresponding peaks. Upper right panel: differential fractionation of the wild-type (WT) and ΔL1 complexes. After inner or outer membrane fractionation as described in Materials and Methods, the complexes were purified and analyzed by SDS-PAGE. “Inner” and “outer” indicate the two gel lanes corresponding to the inner and outer membrane fractions for the WT and ΔL1 complexes, respectively. Lower right panel: localization of the Cys15Ser mutation in the TraN sequence. **B.** Labelling of surface-exposed proteins using Sulfo-NHS-S-S-biotin. In this experiment, expression of *traN-traF*$_{C\text{-}ST}$

(WT) and *traN*$_{Cys15Ser}$-*traF*$_{C\text{-}ST}$ (ΔL1) was induced, cells labelled or not by Sulfo-NHS-S-S-biotin, total membrane proteins extracted, and either directly analysed on SDS-PAGE (left panel) or analysed on SDS-PAGE after neutravidin affinity batch chromatography (right panel). Left panel: Coomassie-staining ("Coomassie") or anti-Strep-tag western blotting ("Anti-strep") of labelled ("NHS-biotin") or unlabelled (∅) membrane proteins separated by SDS-PAGE. This left panel provides the results of the necessary control experiments. Right panel: same as left panel except that the biotin-labelled membrane proteins were purified using neutravidin affinity batch chromatography. The first WT lane in the right panel demonstrates that non-labelled proteins are not pulled down by the neutravidin affinity chromatography. As can be seen in the second WT lane of the panel at right, bands corresponding to the TraF/VirB10 and TraO/VirB9 proteins are clearly present (as assessed visually and also by mass spectrometry analysis of the two bands), indicating either that both proteins are accessible extracellularly or that only one is biotinylated but pulls the other one down because of complex formation. In the ΔL1 complex, the TraO/VirB9 and TraF/VirB10 bands are not visible, indicating that neither TraO/VirB9 nor TraF/VirB10 is accessible extracellularly. We conclude that lipidation of Cys15 of TraN is essential to localize the core T4SS complex to the outer membrane. **C.** Impact of gene deletion on core complex assembly. The four color panels at top provide a schematic diagram of the construct used in this study: ΔTraE/VirB8, ΔTraO/VirB9, ΔL2 ΔTraF/VirB10, and ΔTraN/VirB7, where the *traE*, *traO*, *traF*, or *traN* genes were deleted, respectively (see Materials and Methods). Note that ΔL2 is indistinguishable in composition and structure from the wild-type complex except that ΔL2 does not insert in the outer membrane (Fig. S4, lower panel). The oligomerization state and composition of the complexes of interest were monitored by

gel filtration and Coomassie stained SDS-PAGE and shown in the four panels at bottom for each of the four deletion experiments. The inset within each gel filtration panel shows an SDS-PAGE analysis of the main peak. The complexes were also analyzed by negative stain EM to check for 14-mer ring formation (not shown). This experiment demonstrates that TraE/VirB8 is not involved in 14-mer ring complex formation but that TraN/VirB7, TraO/VirB9, and TraF/VirB10 are.

Fig. S4. Representative class averages (top panel), reprojections (middle panel) and equivalent views of the final maps (bottom panel) for the negative stain EM of the wild-type core complex (NS-WT), negative stain EM of the ΔL2 complex (NS-ΔL2), cryo-EM of the wild-type complex (cryo-WT), the negative stain EM of the D1 complex (NS-D1) and the cryo-EM of the D2 complex (cryo-D2). The lower panel presents a superposition of the negative stain EM structures of the wild-type and ΔL2 complexes, demonstrating the high level of similarity between the two structures.

Fig. S5. Comparison of the EM structures of *E. coli* WzA/WzC and *Salmonella typhimurium* type III secretion injectisome with that of the T4SS core complex. **A.** Type IV secretion core complex (this work). **B.** *E. coli* WzA/WzC EM structure super-imposed with the crystal structure of WzA as in Collins et al. 2007 (*S12*). **C.** Cryo-EM structure of the *Salmonella typhimurium* type III secretion injectisome ΔinJ mutant (*S13*). All structures in A, B, or C, are on the same scale. Also, the positions of the inner (IM) and outer (OM) membranes in these models are indicated. **D.** Docking of the crystal structure of the C-terminal domain of ComB10, a VirB10 homologue. Left panel: side view. Right panel: cut-away side view. Given the strength of the

electron density in the upper part of the outer ring in the O layer, we cannot exclude that this part may contain other structures in addition to the ones already fitted.

Fig. S6. Fourier shell correlation curves of the final models obtained from cryo-EM data (A) and negative stain EM data (B) for the wild-type core complex; from negative stain EM data for the D1 complex (C); from the cryo-EM data for the D2 complex (D); and from the negative stain EM data of the ΔL2 complex (E).

Supplementary Table S1: Oligonucleotides used for cloning

Construct	
IBA3c:*traN-traF*$_{C\text{-}ST}$	5'-ATGGTAGGTCTCAAATGCGCAGCTTATTGCTTATGGGAGT-3'
	5'-ATGGTAGGTCTCAGCGCTGTTGTCTGCGAGCGTATAAACGC-3'
IBA3c:*traN-traO*$_{Ser224Cys}$*-traF*$_{C\text{-}ST}$	5'PHO-TGCGCCAGTGGCAAAGAAACGCTGC-3'
	5'PHO-GATCATGTAGACCTGCGGTAACTCC-3'
IBA3c:*traN*$_{Cys15Ser}$*-traF*$_{C\text{-}ST}$	5'PHO-ATTAGCGCCAGTTCCAGCGGGC-3'
	5'PHO-CAGAAGAACTCCCATAAGCAATAAGCTGC-3'
traN-traF$_{C\text{-}ST}$*(ΔtraN)*	5'PHO-ATGAAAGCTAATAAAAAAACAGGGCTTAC-3'
	5'PHO-TTTTTGCCCTCGTTATCTAGATTTTTGTCG-3'
traN-traF$_{C\text{-}ST}$*(ΔtraE)*	5'PHO-GGGCTGCCCCATGAAAAAACTACTTC-3'
	5'PHO-TTAGCTTTCATTTCGACCACCTTGCG-3'
traN-traF$_{C\text{-}ST}$*(ΔtraO)*	5'PHO-ATGGCCCGTAAAAGTGTCGATGTAGATCAG-3'
	5'PHO-GGGGCAGCCCTCAGTTAACTTCCG-3'
IBA12:$_{OmpA,N\text{-}ST}$*TraN-TraF*	5'-ATGGTAGGTCTCACTCCCATAAACCGCCACCGGAGCCG-3'
	5'-ATGGTAGGTCTCATATCAGTTGTCTGCGAGCGTATAAACGC-3'
IBA12:$_{OmpA,N\text{-}ST}$*TraN-TraF(ΔtraF)*	5'PHO-CGTTTATACGCTCGCAGACAACTAA-3'
	5'PHO-TCAGTTATCCTCCCCAATTTGAACC-3'
IBA3c:*traN*-$_{N\text{-}His}$*traF*$_{C\text{-}ST}$	5'PHO-CACCATCACGCCCGTAAAAGTGTCGATGTAGATC-3'
	5'PHO-ATGGTGATGCATCAGTTATCCTCCCCAATTTGAA-3'

References

S1. J. A. Bradburne, P. Godfrey, J. H. Choi, J. N. Mathis, *Appl Environ Microbiol* **59**, 663 (1993).
S2. M. van Heel, *Ultramicroscopy* **13**, 165 (1984).
S3. J. A. Mindell, N. Grigorieff, *J Struct Biol* **142**, 334 (2003).
S4. S. J. Ludtke, P. R. Baldwin, W. Chiu, *J Struct Biol* **128**, 82 (1999).
S5. M. Van Heel, *Ultramicroscopy* **21**, 111 (1987).
S6. M. van Heel, G. Harauz, E. V. Orlova, R. Schmidt, M. Schatz, *J Struct Biol* **116**, 17 (1996).
S7. E. F. Pettersen *et al.*, *J Comput Chem* **25**, 1605 (2004).
S8. M. Topf *et al.*, *Structure* **16**, 295 (2008).
S9. W. Wriggers, R. A. Milligan, J. A. McCammon, *J Struct Biol* **125**, 185 (1999).
S10. L. Terradot *et al.*, *Proc Natl Acad Sci U S A* **102**, 4596 (2005).
S11. R. Bayliss *et al.*, *Proc Natl Acad Sci U S A* **104**, 1673 (2007).
S12. R. F. Collins *et al.*, *Proc Natl Acad Sci U S A* **104**, 2390 (2007).
S13. T. C. Marlovits *et al.*, *Nature* **441**, 637 (2006).